

Inversion of controlled source audio-frequency magnetotellurics data for a horizontally layered earth

Partha S. Routh* and Douglas W. Oldenburg*

ABSTRACT

We present a technique for inverting controlled source audio-frequency magnetotelluric (CSAMT) data to recover a 1-D conductivity structure. The earth is modeled as a set of horizontal layers with constant conductivity, and the data are apparent resistivities and phases computed from orthogonal electric and magnetic fields due to a finite dipole source. The earth model has many layers compared to the number of data points, and therefore the solution is nonunique. Among the possible solutions, we seek a model with desired character by minimizing a particular model objective function. Traditionally, CSAMT data are inverted either by using the far-field data where magnetotelluric (MT) equations are valid or by correcting the near-field data to an equivalent plane-wave approximation. Here, we invert both apparent resistivity and phase data from the near-field transition zone and the far-field regions in the full CSAMT inversion without any correction. Our inversion is compared with that obtained by inverting near-field corrected data using an MT algorithm. Both synthetic and field data examples indicate that a full CSAMT inversion provides improved information about subsurface conductivity.

INTRODUCTION

Controlled source audio-frequency magnetotellurics (CSAMT) is a frequency-domain electromagnetic method which uses a grounded dipole or horizontal loop as an artificial source. Over the years, CSAMT has emerged as a powerful exploration tool and has found its application in mineral exploration (Zonge et al., 1986; Basokur et al., 1997), geothermal investigation (Sandberg and Hohmann, 1982; Bartel and Jacobson, 1987; Wannamaker, 1997a,b), hydrocarbon exploration (Ostrander et al., 1983) and groundwater contamination problems (Zonge et al., 1985). An excellent

review of CSAMT and its application is given by Zonge and Hughes (1991). The original motivation to develop CSAMT was to improve the signal strength problem that arises in the magnetotelluric (MT) method (Goldstein and Strangway, 1975). However the nonplane wave nature of the source limits the interpretation of data by conventional MT methods. Recognizing this, the traditional practice is to interpret only the far-field data, which are obtained at a distance of four to five skin depths (Sasaki et al., 1992), or to correct near-field data for nonplane-wave effects and then use MT modeling to interpret the observations (Bartel and Jacobson, 1987). The near-field corrections are often based on homogeneous half-space models and their validity is in question in complicated environments. This compromises the information about the subsurface conductivity that can be obtained from transition zone data. Maurer (1988) and Boerner et al. (1993) pointed out the necessity for including complete CSAMT modeling in an inversion and have warned against correcting the data to the plane-wave approximation.

Existing 1-D inversion techniques for CSAMT data (e.g., Zonge and Hughes, 1991) attempt to estimate the conductivities and thicknesses of a few layers by finding the least-square solution of an overdetermined system. Such algorithms concentrate upon reproducing the data, but the resultant model depends upon the number of layers assumed and the initial values of the conductivities and thicknesses. We present an alternative approach by parameterizing the earth into large number of horizontal layers, each of which has a constant, but unknown, conductivity and fixed thickness. The inverse problem becomes underdetermined, and we find a specific model by minimizing a model objective function subject to data constraints. The flexibility of minimizing different model objective functions and fitting the data to different misfits, helps in exploring model space.

The paper begins with a presentation of the forward modeling of CSAMT data in a 1-D earth. Next we discuss the formulation of the inverse problem. We test our inversion with a synthetic data set contaminated with noise. We then apply a

Presented at the 66th Annual International Meeting, Society of Exploration Geophysicists. Manuscript received by the Editor November 12, 1997; revised manuscript received January 29, 1999. Published on Geophysics Online July 7, 1999.

*University of British Columbia, Department of Geophysics and Astronomy, 129-2219 Main Mall, Vancouver, British Columbia V6T 1Z4, Canada.

E-mail: routh@geop.ubc.ca; doug@geop.ubc.ca.

© 1999 Society of Exploration Geophysicists. All rights reserved.

near-field correction and invert the “corrected” data with an MT inversion algorithm. This reinforces the comments made by Maurer (1988) and Boerner et al. (1993). The paper concludes with the inversion of a field data set and a discussion.

THE FORWARD PROBLEM

Forward modeling of CSAMT in one dimension requires the computation of electric and magnetic fields (E_x, E_y, H_x, H_y) over a stratified earth due to horizontal electric dipole (HED). The generic solution of HED is well known (e.g., Wait, 1982; Ward and Hohmann, 1988) and only basic equations need be presented here. We adopt the work of Ward and Hohmann (1988). For a source-free region, the electric and magnetic field can be decomposed in terms of Schelkunoff potential \mathbf{A} and \mathbf{F} , often referred as TM and TE potential. The potential \mathbf{A} is considered to arise from electric sources (J_s) and the \mathbf{F} potential is due to magnetic sources (M_s). The magnetic and electric fields can be expressed in terms of the potentials given by (Ward and Hohmann, 1988),

$$\begin{aligned}\mathbf{H} &= \nabla \times \mathbf{z}A_z(x, y, z, \omega) - (\sigma + i\omega\epsilon)(\mathbf{z}F_z) \\ &\quad + \frac{1}{i\omega\mu} \nabla(\nabla \cdot \mathbf{z}F_z) \\ \mathbf{E} &= -\nabla \times \mathbf{z}F_z(x, y, z, \omega) - (i\omega\mu)(\mathbf{z}A_z) \\ &\quad + \frac{1}{(\sigma + i\omega\epsilon)} \nabla(\nabla \cdot \mathbf{z}A_z)\end{aligned}\quad (1)$$

where \mathbf{z} is the unit vector in the vertical direction, σ is the electrical conductivity, ϵ is the dielectric permittivity, μ is the magnetic permeability, and ω is the angular frequency. Only one component of the vector potential is of interest because the physical properties vary only in one direction. In each source-free layer of constant conductivity (Figure 1), the scalar potential satisfies the following differential equation in the frequency domain (Ward and Hohmann, 1988):

$$\frac{d^2 \tilde{A}_z^j(k_x, k_y, z, \omega)}{dz^2} - u_j^2 \tilde{A}_z^j = 0, \quad (2)$$

$$\frac{d^2 \tilde{F}_z^j(k_x, k_y, z, \omega)}{dz^2} - u_j^2 \tilde{F}_z^j = 0, \quad (3)$$

where $u_j^2 = k_x^2 + k_y^2 - k_j^2$ and $k_j^2 = \omega^2 \mu_j \epsilon_j - i\omega \mu_j \sigma_j$. The A_z and F_z potential at the surface can be expressed as

$$\begin{aligned}A_z^0(x, y, z, \omega) &= \frac{-Ids}{4\pi} \frac{\partial}{\partial x} \int_0^\infty (e^{-u_0(z+h)} \\ &\quad + r_{TM} e^{u_0(z-h)}) \frac{J_0(\lambda r)}{\lambda} d\lambda, \quad (4)\end{aligned}$$

$$\begin{aligned}F_z^0(x, y, z, \omega) &= \frac{-i\omega\mu_0 Ids}{4\pi} \frac{\partial}{\partial y} \int_0^\infty (e^{-u_0(z+h)} \\ &\quad + r_{TE} e^{u_0(z-h)}) \frac{J_0(\lambda r)}{u_0 \lambda} d\lambda, \quad (5)\end{aligned}$$

where $J_0(\lambda r)$ is the Bessel function of zeroth order, $r = \sqrt{x^2 + y^2}$ is the distance from the dipole, h is the height of the dipole above the surface and is equated to zero since the source is at the surface, $u_0 = \sqrt{\lambda^2 - k_0^2}$, $\lambda = \sqrt{k_x^2 + k_y^2}$, and $k_0^2 = \omega^2 \mu_0 \epsilon_0$; r_{TM} and r_{TE} are the TM mode and TE mode reflection coefficients, respectively. The electric field (E_x) and the magnetic

field (H_y) recorded at the surface due to an x -directed HED are expressed in terms of potentials:

$$\begin{aligned}E_x(z=0, \omega) &= \frac{1}{i\omega\epsilon_0} \frac{\partial^2 A_z^0}{\partial x \partial z} - \frac{\partial F_z^0}{\partial y}, \\ H_y(z=0, \omega) &= -\frac{\partial A_z^0}{\partial x} + \frac{1}{i\omega\mu_0} \frac{\partial^2 F_z^0}{\partial y \partial z}.\end{aligned}\quad (6)$$

In practice a long grounded wire is used as a transmitter. It is typically 1–2 km long, whereas the receiver dipole length ranges from 50 to 200 m. The magnetic fields are measured using magnetic sensors (Zonge and Hughes, 1991). The fields due to a point dipole are integrated over the transmitting dipole to find the value at the center of the receiving dipole. The CSAMT data are generally converted to apparent resistivity (ρ_a) and phase (Φ) as a function of frequency. The relationships are

$$\rho_a(z=0, \omega) = \frac{1}{\omega\mu} \left| \frac{E_x(z=0, \omega)}{H_y(z=0, \omega)} \right|^2, \quad (7)$$

$$\phi_a(z=0, \omega) = \phi_{E_x}(z=0, \omega) - \phi_{H_y}(z=0, \omega),$$

where E_x and H_y are the integrated fields due to a finite long grounded wire.

CSAMT data for a five-layer earth model is shown in Figure 2. The transmitter is 1.5 km in length, and the receiving dipoles are parallel to the transmitter but offset by 2 km.

FIG. 1. The conductivity structure for a horizontally-layered earth model: h_j is the thickness of the j th layer, and z_j and σ_j are, respectively, the depth to the bottom and conductivity of the j th layer.

The conductivity structure used to compute the data is shown in Figure 2b, and apparent resistivities and phases are given in Figures 2c–d. It is instructive to compare these responses with MT responses. There is agreement at higher frequencies, but disagreement is pronounced at lower frequencies when nonplane-wave effects become important. The nature of the nonplane-wave effect depends on various factors: frequency of the signal, transmitter-receiver separation, length of the transmitter, orientation of the transmitter and receiver dipoles, and the overall conductivity which alters the skin depths at a particular frequency. The relative contribution of each of these factors to the nonplane-wave effect is difficult to determine since the conductivity structure is unknown. The region around the transmitter is generally divided into three zones. In the near-field region where $r \ll \delta$ (the skin depth), the magnitude of E decays as $1/r^3$ and that of H decays as $1/r^2$, resulting in an E/H which is independent of frequency but dependent on r . This results in the linear decrease in apparent resistivity with increasing frequency on a log-log plot, as shown in Figure 2c. The phase response, shown in Figure 2d, tends to zero. In the region where $r \approx \delta$, the decay of the H -field changes from $1/r^2$ to $1/r^3$; this is called the transition zone. For a layered earth, the transition zone is characterized by a notch, which lies in the frequency range around 100 Hz for this example. The inflection of the phase curve is also indicative of the transition zone response shown in Figure 2d. It has been pointed out (Boerner and West, 1989) that data acquired in the transition zone are generally sensitive to layered structure. The far-field region is characterized by plane-wave behavior of the source and occurs when $r \gg \delta$. In this region, the CSAMT response is same as the MT response.

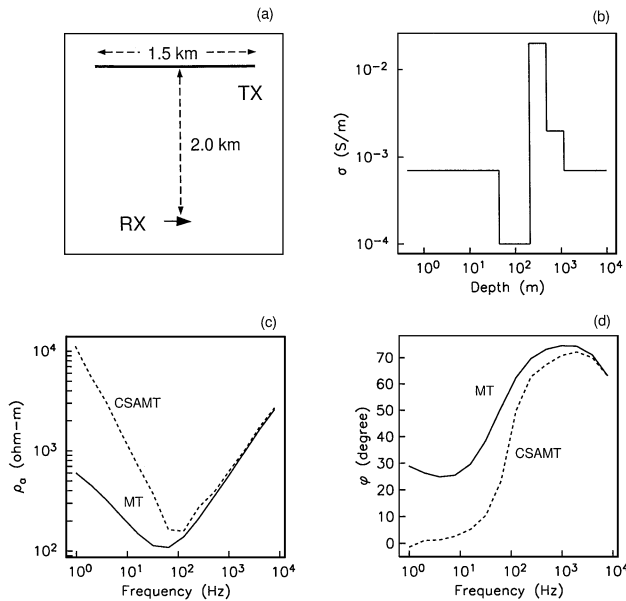


FIG. 2. (a) The transmitter and receiver configuration used to generate the synthetic data. (b) The five-layer true conductivity model used to generate the data. The half-space conductivity at depth is 7.0 mS/m. (c) The CSAMT (dashed line) and MT (solid line) apparent resistivity curve for the five-layer conductivity model. The transition zone notch is observed around 100 Hz on the CSAMT curve. (d) The phase response for CSAMT (dashed line) and MT (solid line).

INVERSE PROBLEM

A primary objective in an inverse problem is to recover a geologically interpretable model that can acceptably reproduce a finite set of observations. The data in a 1-D CSAMT problem are apparent resistivities and phases at frequencies $f_j, j=1, \dots, N$. At each sounding location, the data vector can be represented as $\mathbf{d} = (\rho_a(f_1), \rho_a(f_2), \dots, \rho_a(f_N), \phi(f_1), \phi(f_2), \dots, \phi(f_N))^T$. The medium is discretized into horizontal layers of constant conductivity with increasing layer thickness. To ensure positivity and also to allow large variations of conductivity we choose $m_j = \ln(\sigma_j)$ as our parameters. The model for the inverse problem is $\mathbf{m} = (m_1, m_2, \dots, m_M)$.

For a finite number of inaccurate observations, there are infinite number of solutions that will reproduce the data to within their error. We solve our inverse problem in a standard way by minimizing a model objective function subject to adequately fitting the data. A regularized Gauss-Newton methodology (Constable et al., 1987; Oldenburg et al., 1993) is implemented to iteratively solve the nonlinear optimization problem.

We choose a generic model objective function that is a combination of smallest and flattest model penalty terms:

$$\phi_m = \alpha_s \int_0^\infty w_s(z)(m(z) - m_{ref}(z))^2 dz + \alpha_z \int_0^\infty w_z(z) \left(\frac{dm(z)}{dz} \right)^2 dz, \quad (8)$$

where m_{ref} is the reference model, α_s and α_z are the parameters that control the relative importance of closeness to the reference model and the roughness, and $w_s(z)$ and $w_z(z)$ are additional weighting functions which can be used to control the structural information in the model. Incorporating the layered earth representation into equation (8) allows us to formulate the inverse problem as

$$\begin{aligned} \text{minimize } \phi_m &= \alpha_s \|W_s(\mathbf{m} - \mathbf{m}_{ref})\|^2 + \alpha_z \|W_z \mathbf{m}\|^2 \\ \text{subject to } \phi_d &= \|W_d(\mathbf{d}^{obs} - \mathbf{d}^{pred})\|^2 = \phi_d^*, \end{aligned} \quad (9)$$

where W_s and W_z are finite difference model weighting matrices, ϕ_d^* is the final target misfit to be attained in the inversion process, and W_d is $2N \times 2N$ data weighting matrix. If the data errors are unbiased, independent, and Gaussian, then W_d is a diagonal matrix containing the reciprocals of standard deviations of the data, and ϕ_d is a χ^2 random variable. If such is the case, then the expected value of ϕ_d is equal to $2N$. The inverse problem given in equation (9) can be solved by minimizing a global objective function given by

$$\Phi(m) = \phi_m + \beta^{-1}(\phi_d - \phi_d^*), \quad (10)$$

where β is the regularization parameter. Let us represent the nonlinear mapping between the data and the model by $\mathbf{d} = \mathcal{F}(\mathbf{m})$. Our optimization problem is nonlinear and must be solved iteratively. Let $\mathbf{m}^{(n)}$ be the current model and $\delta \mathbf{m}$ be a perturbation. The forward mapping operator is linearized by a Taylor's series expansion about $\mathbf{m}^{(n)}$ which yields

$$\mathcal{F}(\mathbf{m}^{(n)} + \delta \mathbf{m}) = \mathcal{F}(\mathbf{m}^{(n)}) + J \delta \mathbf{m} + \mathcal{O}(\|\delta \mathbf{m}\|^2), \quad (11)$$

where $\mathcal{O}(\|\delta\mathbf{m}\|^2)$ contains the terms including the second and higher order derivatives with respect to $\delta\mathbf{m}$. J is the sensitivity matrix of order $2N \times M$ with elements $J_{ij} = \partial d_i / \partial m_j$. Neglecting the second and higher order derivatives in equation (11), the perturbed objective function can be written as

$$\begin{aligned} \Phi(\mathbf{m}^{(n)} + \delta\mathbf{m}) &= \alpha_s \|W_s(\mathbf{m}^{(n)} + \delta\mathbf{m} - \mathbf{m}_{ref})\|^2 \\ &+ \alpha_z \|W_z(\mathbf{m}^{(n)} + \delta\mathbf{m})\|^2 \\ &+ \beta^{-1} \left\{ \|W_d(\mathbf{d}^{(obs)} - \mathbf{d}^{(n)} - J\delta\mathbf{m})\|^2 - \phi_d^* \right\}. \end{aligned} \quad (12)$$

The minimum of this perturbed objective function is found by differentiating equation (12) with respect to $\delta\mathbf{m}$ and equating it to zero. This generates a system of M equations in M unknowns given by

$$\begin{aligned} (J^T W_d^T W_d J + \beta W_m^T W_m) \delta\mathbf{m} &= J^T W_d^T W_d \delta\mathbf{d} \\ &- \beta W_m^T W_m \mathbf{m}^{(n)} + \beta \alpha_s W_s^T W_s \mathbf{m}_{ref}, \end{aligned} \quad (13)$$

where $W_m^T W_m = \alpha_s W_s^T W_s + \alpha_z W_z^T W_z$. The system in equation (13) is solved for $\delta\mathbf{m}$. The new model at the $(n+1)$ th iteration is given by $\mathbf{m}^{(n+1)} = \mathbf{m}^{(n)} + \delta\mathbf{m}$, and the new misfit is given by

$$\phi_d^{NL} = \|W_d(\mathbf{d}^{obs} - \mathbf{d}(\mathbf{m}^{(n+1)}))\|^2. \quad (14)$$

The value of β is adjusted using a line search, until the solution of equation (13) generates a misfit of $\phi_d^{NL} = \phi_d^{*(n)}$ where $\phi_d^{*(n)}$ is the target misfit at the n th iteration. The search is continued until ϕ_d^{NL} is close enough to ϕ_d^* or a minimum misfit is found if the target cannot be achieved. The level of desired misfit at each iteration can be chosen based on a simple scheme: $\phi_d^{*(n+1)} = \max\{\zeta \phi_d^{*(n)}, 2N\}$, where $2N$ is the total number of observations and $0 \leq \zeta < 1.0$.

To solve the inverse problem, it is required to compute the sensitivities $J_{ij} = \partial d_i / \partial m_j$ in equation (13). The sensitivities are computed using the adjoint Green's function method (McGillivray and Oldenburg, 1990; Farquarson and Oldenburg, 1993).

INVERSION OF SYNTHETIC DATA

As a test, we apply the inversion algorithm to synthetic CSAMT data obtained from a five-layer conductivity model shown in Figure 2b. The transmitter and receiver dipoles are shown in Figure 2a, and apparent resistivity and phase data were computed at 14 discrete frequencies (1–8192 Hz) yielding 28 data points. The apparent resistivity data were contaminated with Gaussian noise having a standard deviation of 5% of the datum value (apparent resistivity) and 2° for the phase data. The model objective function is

$$\begin{aligned} \phi_m &= \alpha_s \int (\ln \sigma(z) - \ln \sigma_{ref}(z))^2 d \ln(z) \\ &+ \alpha_z \int \left(\frac{d \ln \sigma(z)}{d \ln(z)} \right)^2 d \ln(z), \end{aligned} \quad (15)$$

which is discretized as a layered model in Figure 1. The integral in Equation (15) is taken with respect to $\ln(z)$. This is a natural choice for electromagnetic diffusive problems in which

the frequencies for the data are logarithmically spaced. Equation 15 is the same as equation (8) with $w_s(z) = 1/z$, $w_z(z) = z$, and $m = \ln(\sigma(z))$. Discretizing the first term in equation (15) results in a $M \times M$ weighting matrix for the smallest model shown in Appendix A. This is given by

$$W_s = \text{diag} \left(\sqrt{\frac{h_1}{z_0}}, \sqrt{\frac{h_2}{z_1}}, \dots, \sqrt{\frac{h_{M-1}}{z_{M-2}}}, \sqrt{\frac{h_{M-1}}{z_{M-1}}} \right), \quad (16)$$

where z_i is the depth to the i th interface and h_i is the thickness of i th layer; $z_0 = \xi * h_1$ with $0 < \xi \leq 1$. Discretizing the second term in equation (15) results in an $(M-1) \times M$ weighting matrix for the flattest model shown in Appendix A. This is given by

$$W_z = \begin{pmatrix} -\gamma_1 & \gamma_1 & \cdots & 0 \\ \vdots & \vdots & \vdots & \vdots \\ 0 & 0 & -\gamma_{M-1} & \gamma_{M-1} \end{pmatrix}, \quad (17)$$

where $\gamma_j = \sqrt{(z_j + z_{j-1}) / (h_j + h_{j+1})}$. The choice of z_0 is the same as for the smallest model.

The earth was parameterized into 50 layers with the layer thickness increasing exponentially with depth. The reference model is chosen to be 7×10^{-4} S/m, which is the same as the true background conductivity, and the target misfit at each iteration was halved (i.e., $\zeta = 0.5$) as the iterative process continued. We carry out the inversions using two different objective functions: (1) $\alpha_s = 1.0$, $\alpha_z = 0$, and (2) $\alpha_s = 0$, $\alpha_z = 1.0$. We refer to models obtained from minimizing these objective functions as the smallest and flattest model, respectively. The fits to the observed apparent resistivity and phase for both smallest and flattest models are shown in Figures 3b and 3c. The final misfit for the smallest model and flattest models were 27.8 and 28.0, respectively. The smallest model shown in Figure 3a delineates the boundaries of the conductive layer, but it exhibits more structure than the flattest model, which is a smooth version of the true model. The difference in the two models is seen in the recovery of the background conductivity at larger depth. This occurs because the reference conductivity is chosen to be the true background conductivity. The flattest model penalty term does not have any information about the reference model and, therefore, the model flattens out at depths which are not sensed by data.

The next objective was to invert only one set of information (i.e., either apparent resistivity or phase). In practice, this is sometimes necessary because one of these data sets does not exist, or one is contaminated with severe noise and must be discarded. We first invert only the apparent resistivity data contaminated with noise. The desired misfit in this case is 14. The constructed smallest and flattest models are shown in Figure 4a, and the fit to the data is shown in Figure 4c. The final misfits for the smallest and the flattest models are 13.9 and 14.0, respectively. The flattest model has slightly less structure than that in Figure 3a, but the smallest model has considerably more structure. Inverting only phase data produces the models in Figure 4b, and similar conclusions hold. The fit to the data is shown in Figure 4d. In the inversion with the flattest model objective function where $\alpha_s = 0$, there is no influence of reference conductivity on the inversion. However, it is still possible to recover the conductivity. This arises because the phase data

obtained in the near-field and transition zone change with the frequency and conductivity.

The results in Figure 4 show that conductivity information can be obtained from either amplitude or phase information, but having both data sets improves the inversion result. The degree of improvement depends on the data errors and is also problem dependent. In all three cases, the flattest model recovers a smoother version of the true model, whereas the smallest model shows more structure. A flattest model may be more appropriate in cases where reference conductivity information is not known a priori.

MT INVERSION OF NEAR-FIELD CORRECTED DATA

It is a common practice to invert CSAMT data by first removing the near-field effects and then inverting the data using an MT inversion code. We carry out this procedure to illustrate the advantage of working with fully modeled CSAMT data. In this section, we present the inversion of near-field corrected data using the scheme outlined by Bartel and Jacobson (1987). Following Bartel and Jacobson, two half-space conductivities σ_1 and σ_2 are chosen such that at frequency f

the apparent resistivity of the CSAMT response is bounded between the two homogeneous half-space responses, that is, $\rho_{a1}^{CSAMT}(f) \leq \rho_{am}^{CSAMT}(f) \leq \rho_{a2}^{CSAMT}(f)$. The next step is to use Bartel and Jacobson's equation (3) to compute the near-field corrected apparent resistivity given by

$$\begin{aligned} \log(\rho_{NFC}(f)) &= \frac{[\log(\rho_{am}^{CSAMT} / \rho_{a1}^{CSAMT}) \log(\rho_{a2}^{MT} / \rho_{a1}^{MT})]}{\log(\rho_{a2}^{CSAMT} / \rho_{a1}^{CSAMT})} \\ &+ \log(\rho_{a1}^{MT}), \end{aligned} \tag{18}$$

where the subscript "NFC" denotes the near-field corrected value of apparent resistivity. Unfortunately there is no correction for phase data. This occurs for two reasons. First, the phase at low frequency for CSAMT tends to be small because the notion of frequency sounding breaks down and apparent resistivity depends on the geometry. Second, the half-space technique that works for correcting the apparent resistivity is not applicable since the phase of the MT response for a homogeneous half-space is $\pi/4$ irrespective of the frequency or conductivity.

The important question to be asked in most near-field corrections is which data belong to the near-field and which belong to the transition zone? This is often difficult to judge since the relative contributions of the various factors are unknown. However, from theoretical modeling and characteristic features of the curves (like the transition zone notch), one can select frequencies which seem to be affected by the nonplane-wave

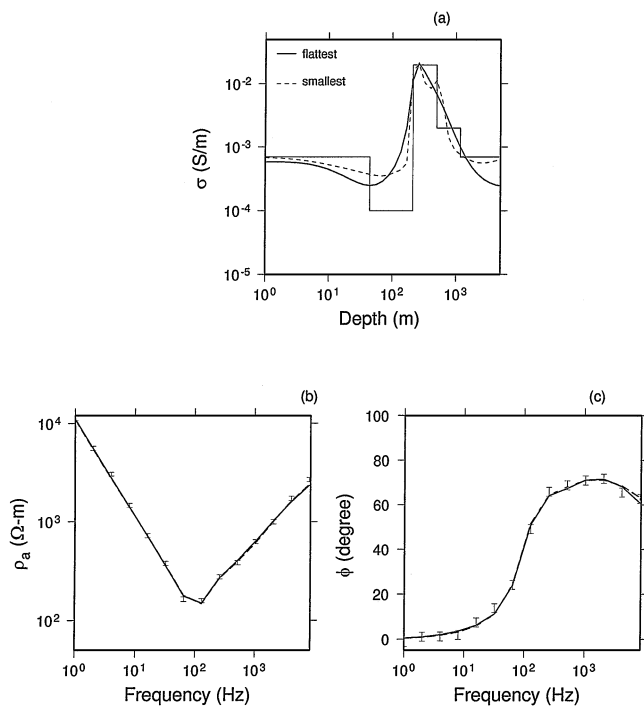


FIG. 3. (a) The recovered models from the simultaneous inversion of apparent resistivity and phase data. The blocky model is the true model, and the flattest model and the smallest model are shown by solid and dotted lines, respectively. For clarity the individual layers are not shown. (b) The synthetic apparent resistivity data and associated error bars generated from the five-layer model. Gaussian random noise with 5% standard deviation of the generated datum value has been added to the data. The predicted data from the smallest and flattest models are shown by continuous and dashed curves, and are indistinguishable. (c) The synthetic phase data and associated error bars generated from five-layer model. Gaussian random noise having 2° standard deviation was added to the synthetic data. The predicted data from the smallest and flattest models are shown by continuous curves.

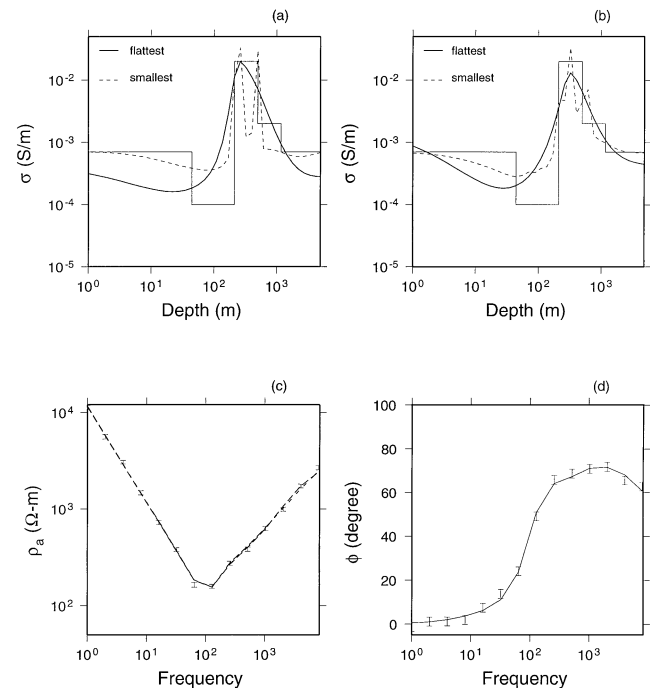


FIG. 4. (a) The recovered model from the inversion of apparent resistivity data. The blocky model is the true model. The flattest and smallest models are shown by solid and dashed lines, respectively. (b) The recovered model from the inversion of phase data. The flattest and smallest models are shown by solid and dashed lines, respectively. (c) The fit to the apparent resistivity data from the smallest and flattest models. (d) The fit to the phase data from the smallest and flattest models.

nature of the source. The apparent resistivity data generated by the model in the last section shows a transition zone notch around 100 Hz. Therefore, the data obtained for frequencies lower than 128 Hz were corrected using equation (18). The near-field corrected apparent resistivity, the CSAMT data, and the computed MT response for the true model are shown in Figure 5b. The data for inversion consists of 14 apparent resistivities including the 10 near-field corrected data and 4 phase data in the far-field region. The errors in apparent resistivity data are assumed to be 5% of the datum value and 2° for the phase. The data are inverted using an MT algorithm (Dosso and Oldenburg, 1989) with a target χ^2 of 18 for a flattest model. The resulting model is shown in Figure 5a. Next, the CSAMT inversion was carried out with 14 apparent resistivity data and 14 phase data. The resulting model for the flattest model penalty is superimposed on the MT inversion results for comparison. Although the model objective function for the two inversions is identical, there is an erroneous higher conductive feature observed at greater depth in the near-field corrected inversion. This is probably due to under corrections of the data in the transition zone.

In a more extreme example, we consider a conductive overburden model with a conductive layer in a resistive basement shown in Figure 5c. We keep the same geometry of receiver and

transmitter as that of previous case. The CSAMT response, the MT response, and near-field corrected response are shown in Figure 5d. Unlike the previous case (Figure 5a), the response is mostly obtained in the near-field zone and perhaps in the transition zone. This is probably due to a more resistive basement than in the previous example. The inverted models obtained by minimizing a flattest model objective function are shown in Figure 5c. The deeper conductive layer is totally absent in the near-field corrected inversion using MT, whereas it is clearly visible in the CSAMT inversion.

FIELD DATA INVERSION

A goal of our research is to develop an algorithm which produces an interpretable electrical conductivity model when applied to field data. In practice, geophysical surveys are likely affected by 3-D conductivity. Therefore, the validity of using 1-D algorithm to invert 3-D data can be in question, but this is not the issue we are trying to address in this paper. Wannamaker (1997b) and Boschetto and Hohmann (1991) have examined the discrepancy between the 1-D and 3-D modeling results with CSAMT. Our goal here is to present a robust inversion algorithm that can be applied to field data when the earth is approximately 1-D. We present one example of inverting field data and compare our results with near-field corrected 1-D MT inversion obtained from a commercial contractor.

In CSAMT, the data at low frequencies that contain the deeper information are often contaminated with the near-field effects. Therefore, the goal of this example is to investigate the usefulness of CSAMT inversion in a conductive environment when information about the deeper subsurface is desired. Our data set was acquired during a mineral exploration survey in Nevada. The observed apparent resistivity and phase data are presented in Figure 6a and Figure 6c, respectively. The data were collected using a transmitter of length 7450 ft (2270 m) placed 14 800 ft (4500 m) from the receiving dipoles. The transmitting dipole is parallel to the receiver dipoles. The receiving dipoles are separated by 100 ft (30 m) along the survey line. Data at 13 frequencies (0.5–2048 Hz) were acquired at 60 locations. Near-field effects, which cause the resistivity to increase and phase to decrease with decreasing frequency, are observed in the low-frequency regime shown in Figures 6a and 6c. If a 1-D assumption is valid, we expect the data to vary smoothly from site to site. The phase data in Figure 6c do that, except in the region between 2000 and 3000 ft, where there is an obvious anomaly. The resistivity data in Figure 6a show somewhat more variation from site to site, which could be due to static shifts caused by surface conductors. We do not apply any static shift correction prior to inverting the data.

To invert the data, we assigned a 10% error to apparent resistivities and a 5° error on the phases. The target misfit was set to 26, which is equal to the number of data. We could reach the desired target misfit of 26 for all the stations. The model objective function chosen for inverting the data is a combination of smallest and flattest component ($\alpha_s = 0.0001$ and $\alpha_z = 1$). The reference model is a homogeneous half-space of 0.01 S/m. The model obtained from inversion is presented in Figure 7a. The recovered conductivity indicates a resistive anomaly near 2800 ft. The regional structure indicates a near-surface conducting layer with a resistive basement. The shallow depth information is mostly obtained from the high-frequency data,

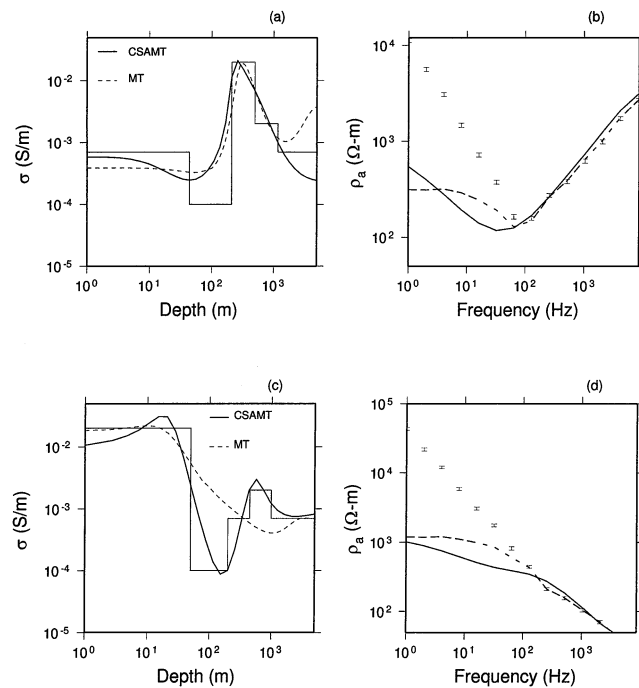


FIG. 5. (a) The recovered model from the CSAMT inversion (solid line) and the model from the MT inversion of near-field corrected data (dashed line). The block model is the true model. (b) The computed MT apparent resistivity for the true model in (a) is shown as a solid line. The generated CSAMT responses with receiver at (0, 2 km) from the center of the transmitter are shown with error bars. The dashed line indicates the near-field corrected data. (c) The block solid line is the true model. The CSAMT inversion and the MT inversion of near-field corrected data is indicated by solid and dashed lines, respectively. (d) The computed MT apparent resistivity for the true model in (c) is shown by a solid line. The CSAMT responses are shown with error bars, and the dashed line indicates the near-field corrected data.

which lies in the far-field region. The deeper information is obtained from the near-field data collected at low frequencies. Figures 6b and 6d indicate a good match between the predicted and the observed data. Because of the concern regarding static shift of apparent resistivities, we also inverted the data by downweighting the apparent resistivity values. This was done by assigning an error of 20% to the resistivity data and 5° error to the phases. The conductivity model obtained was very similar, but slightly smoother, than that obtained in Figure 7a.

Next we compare the CSAMT inversion with the 1-D MT inversion of near-field corrected data. For comparison, we consider the top 4000 ft (1200 m) of recovered model obtained from CSAMT inversion and compare it with the near-field corrected inversion shown in Figure 7b. The conductivity structure in the upper part of the model indicates a shallow conductive layer which agrees well with that obtained from CSAMT inversion (Figure 7a). However, there are several differences in the deeper structures as well as in the recovered amplitudes. The amplitude of the resistive anomaly obtained at 2800 ft from CSAMT inversion is higher than that obtained from the near-field corrected data. The CSAMT inversion shown in Figure 7a indicates a gently dipping resistive basement, whereas the near-field corrected data shows more structure in the deeper section. In general, there is a reasonable agreement between the two inversions (Figures 7a and 7b) at shallower depths. This is because the data obtained at higher frequencies lie in the far-field zone where the plane wave approximation is valid. However, the agreement worsens at depth, which is

probably due to the near-field corrections applied to the low-frequency data.

Some qualitative information about the conductivity can be obtained from drillhole logs BH1 and BH2 shown in Figures 8b and 8c, respectively. The locations of the drillhole logs on the inverted model are presented in Figure 8a. BH1 penetrates the resistive block, and BH2 intersects the surface conductive layer. The BH1 log shown in Figure 8b indicates that the top alluvium layer is underlain by more resistive siltstone and sandstone units. The rock type where the resistive block is encountered is predominantly siltstone with fine-grained sandstone. A few quartz veins with silicified siltstone are also found in this region, consistent with the high resistivity obtained from the inversion. The drillhole information in BH2 indicates that the top layer is alluvium followed by clay and siltstone. In the depth range of 470–710 ft (143–216 m), there is clay-rich layer with occurrences of siltstone and iron oxide that is relatively conductive. Although there are no geophysical logs available in this region, the high-resistive block and the shallow-conductive layer obtained in our inversion are a qualitative indicator of the rock type assemblage found in the two drillhole logs BH1 and BH2.

CONCLUSION

There are two reasons for not interpreting “corrected” CSAMT data with a MT inversion algorithm: (1) inappropriate correction of the near-field and transition zone data can generate artifacts in the inversion results, (2) the corrections are only

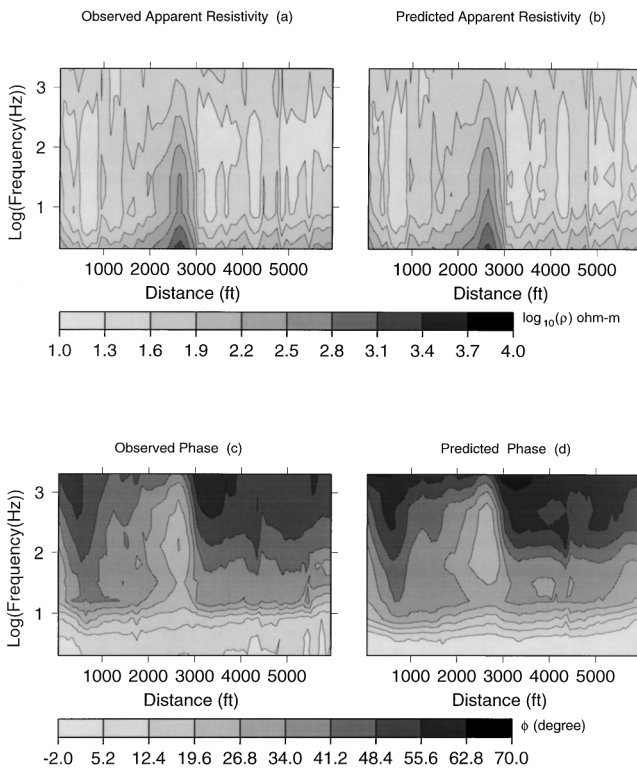


FIG. 6. (a) The observed apparent resistivity data for field data collected in a conductive environment. (b) The observed phase data. (c) The predicted apparent resistivity data from CSAMT inversion. (d) The predicted phase data from CSAMT inversion.

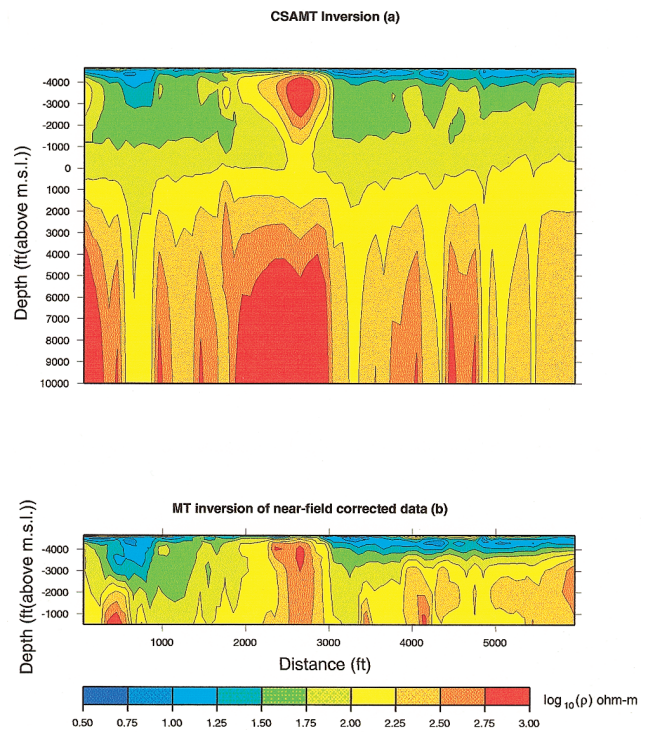


FIG. 7. (a) Resistivity model obtained from CSAMT inversion of the data. Zero on the depth scale indicates the mean sea level. (b) Inverted model obtained from MT inversion of near-field corrected data obtained from commercial processing.

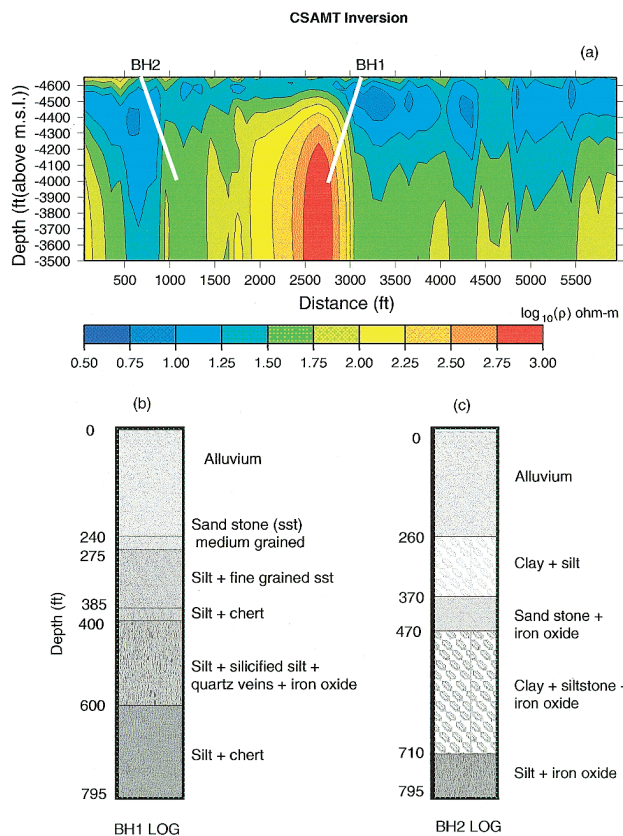


FIG. 8. (a) Resistivity model obtained from CSAMT inversion for top 1150 ft (350 m) above mean sea level. The drillhole logs are superimposed on the inverted section. (b) The rock type assemblage in BH1. The drillhole is 795 ft (242 m) long and penetrates the resistive block. (c) The rock type assemblage in BH2.

applied to resistivity data and the phase data, which cannot be corrected, must be discarded while carrying out MT inversion. In this paper, we have developed an inversion algorithm to recover a 1-D conductivity structure from CSAMT data without applying any correction prior to inversion. The forward modeling is carried out in the frequency domain, and sensitivities are computed using an adjoint Green's function. The inversion method finds a particular model by minimizing a model objective function subject to adequately fitting the data. Here, we confine ourselves to models that are smooth vertically and are also close to a reference model. Resistivity and phase data can be inverted jointly or separately. Results from our inversion are compared with those obtained by applying an MT inversion algorithm to near-field corrected data. Significant differences in the conductivity models are obtained in both synthetic and field data examples, and these differences illustrate the need to invert CSAMT data without any correction.

ACKNOWLEDGMENTS

We thank Dick West of BHP Minerals for providing the CSAMT data set. The critical reviews of Greg Newman, Michael Oristaglio, Randy Mackie, Martyn Unsworth, and an anonymous reviewer helped to improve the paper. This work was supported by NSERC IOR grant 5-81215 and an industry

consortium, "Joint and Cooperative Inversion of Geophysical and Geological Data." Participating companies are Placer Dome, BHP Minerals, Noranda Exploration, Cominco Exploration, Falconbridge Limited (Exploration), INCO Exploration and Technical Services, Hudson Bay Exploration and Development, Kennecott Exploration, Newmont Gold Company, WMC, and CRA Exploration.

REFERENCES

- Bartel, L. C., and Jacobson, R. D., 1987, Results of a controlled-source audiofrequency magnetotelluric survey at the Puhimau thermal area, Kilauea Volcano, Hawaii: *Geophysics*, **52**, 665–677.
- Basokur, A. T., Rasmussen, T. M., Kaya, C., Altun, Y., and Aktas, K., 1997, Comparison of induced-polarisation and controlled-source audio-magnetotellurics methods for massive chalcopyrite exploration in a volcanic area: *Geophysics*, **62**, 1087–1096.
- Boerner, D. E., and West, G. F., 1989, A spatial and spectral analysis of the electromagnetic sensitivity in a layered earth: *Geophys. J.*, **98**, 11–21.
- Boerner, D. E., Kurtz, R. D., and Jones, A. G., 1993, Orthogonality in CSAMT and MT measurements: *Geophysics*, **58**, 924–934.
- Boschetto, N. B., and Hohmann, G. W., 1991, Controlled-source audiofrequency magnetotelluric responses of three-dimensional bodies: *Geophysics*, **56**, 255–264.
- Constable, S. C., Parker, R. L., and Constable, C. G., 1987, Occam's inversion: A practical algorithm for generating smooth models from electromagnetic sounding data: *Geophysics*, **52**, 289–300.
- Dozzo, S. E., and Oldenburg, D. W., 1989, Linear and non-linear appraisal using extremal models of bounded variation: *Geophys. J. Internat.*, **99**, 483–495.
- Farquarson, C. G., and Oldenburg, D. W., 1993, Inversion of time-domain electromagnetic data for a horizontally layered earth: *Geophys. J. Internat.*, **114**, 433–442.
- Goldstein, M. A., and Strangway, D. W., 1975, Audio-frequency magnetotellurics with a grounded electric dipole source: *Geophysics*, **40**, 669–683.
- Maurer, H. M., 1988, Discussion on: "Results of a controlled-source audiofrequency magnetotelluric survey at the Puhimau thermal area, Kilauea Volcano, Hawaii," Bartel, L. C., and Jacobson, R. D., authors: *Geophysics*, **53**, 724–725.
- McGillivray, P. R., and Oldenburg, D. W., 1990, Methods for calculating Fréchet derivatives and sensitivities for the non-linear inverse problem: a comparative study: *Geophys. Prosp.*, **38**, 499–524.
- Oldenburg, D. W., McGillivray, P. R., and Ellis, R. G., 1993, Generalized subspace methods for large-scale inverse problems: *Geophys. J. Internat.*, **114**, 12–20.
- Ostrander, A. G., Carlson, N. R., and Zonge, K. L., 1983, Further evidence of electrical anomalies over hydrocarbon accumulations using CSAMT: 53rd Ann. Internat. Mtg., Soc. Expl. Geophys., Expanded Abstracts, 60–63.
- Sandberg, S. K., and Hohmann, G. W., 1982, Controlled-source audio-magnetotellurics in geothermal exploration: *Geophysics*, **47**, 100–116.
- Sasaki, Y., Yoshihiro, Y., and Matsuo, K., 1992, Resistivity imaging of controlled-source audiofrequency magnetotelluric data: *Geophysics*, **57**, 952–955.
- Wannamaker, P. E., 1997a, Tensor CSAMT survey over the Sulphur Springs thermal area, Valles Caldera, New Mexico, U.S.A., Part I: Implications for structure of the western caldera: *Geophysics*, **62**, 451–465.
- 1997b, Tensor CSAMT survey over the Sulphur Springs thermal area, Valles Caldera, New Mexico, U.S.A., Part II: Implications for CSAMT methodology, *Geophysics*, **62**, 466–476.
- Ward, S. H., and Hohmann, G. W., 1988, Electromagnetic theory for geophysical applications, in Nabighian, M. N., Ed., *Electromagnetic methods in applied geophysics*: Soc. Expl. Geophys.
- Wait, J. R., 1982, *Geoelectromagnetism*: Academic Press Inc.
- Zonge, K. L., and Hughes, L. J., 1991, Controlled source audio-frequency magnetotellurics, in Nabighian, M. N., Ed., *Electromagnetic methods in applied geophysics*, **2**: Soc. Expl. Geophys.
- Zonge, K. L., Ostrander, A. G., and Emer, D. F., 1986, Controlled-source audiofrequency magnetotelluric measurements, in Vozoff, K., Ed., *Magnetotelluric methods*: Soc. Expl. Geophys. Geophysics Reprint Series **5**, 749–763.
- Zonge, K. L., Figgins, S. J., and Hughes, L. J., 1985, Use of electrical geophysics to detect sources of groundwater contamination: 55th Ann. Internat. Mtg., Soc. Expl. Geophys., Expanded Abstracts, 147–149.

APPENDIX A

DERIVATION FOR THE SMALLEST (W_s) AND FLATTEST (W_z) MODEL NORM MATRICES

In a CSAMT survey, data are acquired at frequencies which span several decades (e.g., 0.5–4096 Hz). The corresponding skin depths also span several decades, and so a logarithmic depth spacing is appropriate to discretize the medium for a 1-D earth. We adopt equation (15) as a suitable model objective function to be minimized. Here, we derive the discretized form of the model objective function in equation (15) for the smallest and the flattest model component. The component for the smallest model norm in equation (15) is given by

$$\begin{aligned}\phi_m^s &= \int (m(z) - m_{ref}(z))^2 d \ln z \\ &= \int \left(\frac{1}{z}\right) (m(z) - m_{ref}(z))^2 dz, \quad (\text{A-1})\end{aligned}$$

where $m = \ln \sigma$ is the model. We note that the additional weighting function $w_s(z)$ defined in equation (8) is equal to $1/z$. To prevent effects of singularity in the weighting, we set $w_s(z) = 1/z_0$ when $z \leq z_0$ and where z_0 is a nonzero depth less than the thickness of the first layer. For practical purposes, the upper limit of the integral is evaluated up to z_{\max} , which is chosen to be sufficiently large. For the discrete 1-D model shown in Figure 1, we choose a discrete set of weights for $w_s(z)$. This is given by

$$\begin{aligned}w_s(z) &= \frac{1}{z_0} \quad \text{for } 0 \leq z \leq z_1 \\ &= \frac{1}{z_{j-1}} \quad \text{for } z_{j-1} \leq z \leq z_j; j = 2, \dots, M. \quad (\text{A-2})\end{aligned}$$

Discretizing the integral for an M -layered earth yields

$$\begin{aligned}\phi_m^s &= \sum_{j=1}^M (m_j - (m_{ref})_j)^2 \left(\frac{1}{z_{j-1}}\right) \Delta z_j \\ &= \sum_{j=1}^M (m_j - (m_{ref})_j)^2 \left(\frac{h_j}{z_{j-1}}\right), \quad (\text{A-3})\end{aligned}$$

where $\Delta z_j = z_j - z_{j-1} = h_j$ is the thickness of the j th layer. Equation (A-3) can be rearranged such that it can be written

in the matrix form given by

$$\phi_m^s = \sum_{j=1}^M \left[\sqrt{\left(\frac{h_j}{z_{j-1}}\right)} (m_j - (m_{ref})_j) \right]^2 = m^T W_s^T W_s m. \quad (\text{A-4})$$

Therefore $W_s = \text{diag}(\sqrt{h_j/z_{j-1}})$ for $j = 1, \dots, M$. For the bottom half-space, we choose the thickness to be equal to the thickness of the layer above it (i.e., $h_M = h_{M-1}$). We note that since the layer thickness increases exponentially with depth, the ratio of h_{M-1}/z_{M-1} is finite and on the order of unity. Thus, at greater depths where the data are insensitive to the structure, the inversion recovers the reference model.

The component for the flattest model norm from equation (15) is given by

$$\phi_m^f = \int_0^\infty \left(\frac{dm(z)}{d \ln z}\right)^2 d \ln z = \int_0^\infty z \left(\frac{dm(z)}{dz}\right)^2 dz. \quad (\text{A-5})$$

We note that the additional weighting function $w_z(z)$ defined in equation (8) is equal to z . Discretizing the integral in equation (A-5) for an M -layered model yields

$$\begin{aligned}\phi_m^f &= \sum_{j=1}^{M-1} \left(\frac{z_j + z_{j-1}}{2}\right) \left(\frac{m_{j+1} - m_j}{\frac{\Delta z_{j+1} + \Delta z_j}{2}}\right)^2 \left(\frac{\Delta z_{j+1} + \Delta z_j}{2}\right) \\ &= \sum_{j=1}^{M-1} (m_{j+1} - m_j)^2 \left(\frac{z_j + z_{j-1}}{h_{j+1} + h_j}\right). \quad (\text{A-6})\end{aligned}$$

Equation (A-6) can be rearranged such that it can be written in the matrix form given by

$$\begin{aligned}\phi_m^f &= \sum_{j=1}^{M-1} \left[\sqrt{\left(\frac{z_j + z_{j-1}}{h_{j+1} + h_j}\right)} (m_{j+1} - m_j) \right]^2 \\ &= m^T W_z^T W_z m. \quad (\text{A-7})\end{aligned}$$

This implies that the flattest model norm matrix W_z is a $M-1 \times M$ matrix with the elements shown in Equation (17).